Oil Shale, 2019, Vol. 36, No. 3, pp. 370–391
doi: https://doi.org/10.3176/oil.2019.3.02
ISSN 0208-189X

Synergy analysis for co-pyrolysis of oil shale and shale oil sludge

Qin Hong[(a)], Zhou Lei[(a)], Zhang Lidong[(a)], Liu Hongpeng[(a)], Jia Chunxia[(a)], Wang Qing[(a)]*, Chen Meiduan[(b)]

[(a)] Engineering Research Center of Oil Shale Comprehensive Utilization, Ministry of Education, Northeast Electric Power University, Changchun Road 169, Jilin, 132012, PR China
[(b)] Huaneng Qinbei Power Generation Co. Ltd., Wulongkou Town, Jiyuan city, Henan, 454662, PR China

Abstract. *Shale oil sludge is a hazardous by-product of hydrocarbon production that needs an effective and safe degradation. Co-pyrolysis with oil shale is a promising method to efficiently render the sludge non-toxic. Pyrolysis of the mixture of oil shale and shale oil sludge was studied using a thermogravimetric analyzer (TGA). The synergistic pyrolysis parameters were calculated using the coefficient of mutual influence f and the relative error of the root mean square (RMS). Experiments on co-pyrolysis were conducted through measuring the gaseous product and semi-coke by using an infrared (IR) analyzer, a scanning electron microscope (SEM), an energy dispersive spectrometer (EDS) and a specific surface area (SSA) analyzer separately. Pyrolysis kinetics was obtained by the Coats-Redfern (CR) method. The synergistic analysis showed the increasing sludge content to advance the pyrolysis of the mixed sample during the process. The surface morphology and amount of micropores of the mixture varied with increasing sludge proportion. The activation energy (E) of the mixture was gradually reduced with the degree of the reaction, while it slowly increased as the reaction proceeded to third stage and the frequency factor gradually decreased with the depth of the reaction. Therefore, the co-pyrolysis had an optimum reaction temperature interval and the degree of reaction was related to the chemical reaction between the reactants.*

Keywords: *shale oil sludge, co-pyrolysis kinetics, synergy, specific surface area, activation energy.*

* Corresponding author: e-mail *343762921@qq.com*

1. Introduction

Currently, many industries throughout China are actively engaged in oil shale exploitation [1]. Shale oil sludge, a lipophilic deposit generated during oil shale retorting, contains excessive shale dust absorbed with fine oil mist and water. Generally, shale oil sludge accounts for 3 to 5 percent of shale oil production. Shale oil sludge is difficult to degrade naturally and contaminates soil as well as groundwater when stored on the surface. Due to the high oil content of shale oil sludge, recycling the oil is a solution to the above problems. At present, the major methods for processing shale oil sludge include incineration, pyrolysis, and extraction of the remaining oil by solvent. Pyrolysis may be an ideal solution to the sludge treatment, which can be easily integrated into the current retorting technological process, through directing the collected sludge back into the retort furnace.

The results of many researches show that during the co-pyrolysis of different fuels the reactants interact with each other and promote the process. Peng et al. [2] studied the kinetics and products during the co-pyrolysis of microalgae and textile dyeing sludge and found an obvious positive synergistic interaction to exist between the components during the process. Bičáková and Straka [3] suggested that it was possible to increase the production of tar and coke during the decomposition of bituminous coal when mixing it with a certain amount of waste tires. When conducting experiments on co-pyrolysis of oil shale and low density polyethylene in a fixed bed, Bozkurt et al. [4] found the rate of tar output to be higher than that with oil shale alone. Lin et al. [5] discovered that mixing 10% sewage sludge with oil shale reduced the activation energy (E) of the latter significantly. Bai et al. [6] noticed that when blending oil shale with 50% alkali lignite, the most gaseous products were released, while with 80% alkali lignite in the mixture, the release was the least. Meanwhile, aromatic compounds, phenolic compounds and water were also found to be reduced when 50% alkali lignin was mixed. Liu et al. [7] carried out experiments to seek the effect of municipal sewage sludge on coal distillation and thus revealed the catalytic action on coal decomposition to come from inorganic compounds contained in it. Huang et al. [8] found that sewage sludge absorbed microwave energy more effectively by adding 20% rice straw and thus the maximum temperature reached 500 °C during the sewage sludge pyrolysis in a microwave oven. In addition, some studies have also established that co-pyrolysis significantly improves the yield and quality of liquid and gaseous products [9, 10]. However, to date only few researches on the co-pyrolysis of oil shale and shale oil sludge have been reported.

In this paper, experiments on co-pyrolysis of oil shale and shale oil sludge were carried out with the aim to find out the interrelationship between the reactants during the process. A combination instrument of thermogravimetric analyzer (TGA) was used to determine the pyrolysis characteristics. Correspondingly, the kinetic parameters of co-pyrolysis were calculated

using the Coats-Redfern (CR) method. The pyrolysis gas was measured by the Fourier transform infrared (FTIR) spectrometer connected with TGA. The change of the micromorphology of oil shale after thermal decomposition with shale oil sludge was observed using a scanning electron microscope (SEM) and the variation of micropore structure was measured employing a specific surface area (SSA) analyzer. The results obtained were used to determine the interaction between oil shale and shale oil sludge in the distillation process. In addition, an energy dispersive spectrometer (EDS) was applied to analyze the variation of inorganic minerals on the surface of samples.

2. Experimental

2.1. Material and sample preparation

A mixture of Longkou oil shale received from Shandong Province of China and shale oil sludge obtained during the oil shale retorting was used in various ratios throughout the experiments. Oil shale and shale oil sludge were ground into fine particles (< 0.2 mm) and sieved separately. After sieving, the oil shale and sludge samples were placed into the drying oven at 50 °C for 24 hours to remove the external moisture and sludge environmental moisture. The ground and dried sludge was then mixed with oil shale at various percentages: 0%, 20%, 40%, 60%, 80% and 100% (Table 1).

2.2. Apparatus and methods

The Mettler Toledo TGA/DSC1 thermogravimetric infrared analyzer (Switzerland) was used to analyze the pyrolysis of samples. Approximately 20 mg (±0.5 mg) of each mixture consisting of oil shale and shale oil sludge in various ratios was placed in a crucible inside the instrument. The carrier gas was 99.999% pure nitrogen at a flow rate of 50 ml/min. The test system was purged with nitrogen for 30 min before the experiment to remove any impurity gas from the reaction system. The sample was then warmed from room temperature to 50 °C and held for 10 min to remove excess water. The samples were then heated from 50 °C to 900 °C at a rate of 10, 30 or 50 °C/min.

The gaseous co-pyrolysis product of oil shale and sludge flowed into a gas pool in FTIR spectrometer through a heated transfer tube for real-time detection. When the experimental sample began to decompose, the infrared spectrum started to collect and analyze the gaseous product on a NICOLET IS10 Fourier transform spectrometer. The detector on the NICOLET was DTGS/KBr, and the absorption wavenumber of the FTIR spectrum ranged from 500 to 4000 cm^{-1}.

The microstructure of the pyrolysis products was then analyzed using a tube furnace at different heating rates for 2 mm particles. The pyrolysis products were analyzed by scanning electron microscopy (SEM), energy dispersive spectrometry (EDS) and specific surface area (SSA) analysis.

2.3. Synergy and kinetics theory

The coefficient of mutual error *f* and the relative error of the root mean square (RMS) for the experimental and theoretical values were used to study the mutual influence between the oil shale and shale oil sludge samples in the co-pyrolysis process. With *f* greater than 1, the samples reciprocally enhanced co-pyrolysis. Conversely, co-pyrolysis was mutually inhibited when *f* was smaller than 1. RMS reflects the degree of interaction between the samples. The larger the RMS, the higher the degree of interaction between oil shale and shale oil sludge in the co-pyrolysis process. *f* and RMS are calculated as follows:

$$f = \frac{R_{\exp}\Delta T_{1/2,\exp} / T_{p,\exp}}{R_{cal}\Delta T_{1/2,cal} / T_{p,cal}}, \tag{1}$$

$$RMS = \sqrt{\frac{\sum_{i=1}^{n}\left(\frac{x_{\exp}^{i} - x_{cal}^{i}}{x_{cal}^{i}}\right)^{2}}{n}}, \tag{2}$$

where R is the weight loss peak, %; $\Delta T_{1/2}$ is the half width, °C; T_p is the peak temperature, °C; Xi is the i point weight loss rate, %/min; n is the number of points taken.

Pyrolysis is a complex process of physical and chemical reactions whose chemical reaction rate depends on the concentration and rate constant of the participating reactants. When the reactant concentration is constant, the reaction rate depends only on the reaction rate constant. Methods used for the kinetic analysis of the pyrolysis process include a single scanning rate method and a multiple scanning rate method. Solution methods used for evaluating kinetic parameters are a constant temperature method and a non-constant temperature method. The multiple scanning rate method in turn includes the distributed activation energy model (DAEM), Flynn-Wall-Ozawa (FWO) and Starink methods. The kinetic parameters of pyrolysis of the samples were calculated by the CR method. By using the latter method, the stage of pyrolysis of oil shale and shale oil sludge can be determined. The reaction mechanism can be determined by a simple reaction order equation. The basic equation of the pyrolysis reaction is expressed as follows [11–13]:

$$\frac{d\alpha}{dt} = \frac{A}{\beta}k(T)f(\alpha). \tag{3}$$

In the case of linear heating, $\beta = dT/dt$, the pyrolysis rate equation can be written as:

$$\frac{d\alpha}{dT} = \frac{A}{\beta}k(T)f(\alpha). \tag{4}$$

For the slow heating process of pyrolysis, the reaction rate can be considered to be controlled by chemical motivational factors. The relationship between the reaction rate and the temperature follows the Arrhenius law. The pyrolysis rate equation can be written as:

$$\frac{d\alpha}{dT} = \frac{A}{\beta}\exp(-\frac{E}{RT})f(\alpha), \tag{5}$$

$$\alpha = (m_0 - m_T)/(m_0 - m_f), \tag{6}$$

where α is the conversion rate; A is the pre-exponential factor, min^{-1}; E is the activation energy, kJ/mol; R is the gas constant; $f(\alpha)$ is the reaction mechanism function; m_0, m_T, and m_f are the initial mass of the sample, the mass at which the temperature reaches T and the residual mass of the sample at the end of the reaction, respectively.

By using the Coats-Redfern method, the mechanism formula is:

$$f(\alpha) = (1-\alpha)^n. \tag{7}$$

In this case, the determination of $f(\alpha)$ is transformed into the determination of the reaction order n. The formula for the Coats-Redfern method is [14]:

$$\ln[\frac{G(\alpha)}{T^2}] = \ln(\frac{AR}{\beta E}) - \frac{E}{RT}, \tag{8}$$

where the equation for $G(\alpha)$ is:

$$\ln[\frac{1-(1-\alpha)^{1-n}}{T^2(1-n)}] = \ln\{\frac{AR}{\beta E}[1-\frac{2RT}{E}]\} - \frac{E}{2.3RT}_{(n\neq 1)}, \tag{9}$$

$$\ln[\frac{-\ln(1-\alpha)}{T^2}] = \ln\{\frac{AR}{\beta E}[1-\frac{2RT}{E}]\} - \frac{E}{2.3RT}_{(n=1)}. \tag{10}$$

The reaction orders calculated are 1/3, 2/3, 0.5, 1, 1.5, 2, 2.5, 3, 3.5, 4, 4,5, 5, 5.5, 6, 6.5, 7, 7.5, 8, 8.5, 9, 9.5 and 10. Think of $1/T$ as X and a linear regression for the left side of Equation (11) or (12) with $1/T$. Each sample selects the reaction order n when the fitting coefficient is the highest, and then the activation energy E and the pre-exponential factor A can be obtained according to the slope and the intercept.

Table 1 gives the proportions of mixture components and Table 2 presents the results of proximate and ultimate analyses of oil shale and shale oil sludge.

Table 1. Proportions of mixture components

Sample / Mixture	S_1	S_2	S_3	S_4	S_5	S_6
SS:OS	0:10	2:8	4:6	6:4	8:2	10:0

SS – shale oil sludge; OS – oil shale.

Table 2. Ultimate and proximate analyses of oil shale and shale oil sludge samples

Sample	Ultimate analysis					Proximate analysis			
	C	H	O	N	S	M	A	V	FC
OS	31.09	3.134	0.82	8.70	0.656	2.29	53.31	30.39	14.01
SS	42.60	6.838	5.946	0.876	0.659	9.86	33.22	47.98	8.94

OS – oil shale; SS – shale oil sludge; C – carbon; H – hydrogen; O – oxygen; N – nitrogen; S – sulfur; M – moisture; A – ash; V – volatile; FC – fixed carbon.

3. Results and discussion

3.1. Pyrolysis of pure sample

Figure 1 shows the thermogravimetric-differential thermogravimetric (TG-DTG) curves of pyrolysis of oil shale (Fig. 1a) and shale oil sludge (Fig. 1b) at 10 °C/min. The pyrolysis of oil shale can be divided into two stages (Fig. 1a). In the first stage, a small weight loss below 200 °C was due to the drying process of oil shale. In the low temperature range, between 380 °C and 620 °C, there took place mainly the volatile gas overflow caused by the oil shale weight loss during pyrolysis. This low temperature stage was the main phase of oil shale pyrolysis and consisted predominantly of the decomposition of hydrocarbon compounds and production of abundant volatiles. The second stage encompassed the high temperature region of 620–900 °C and mainly consisted of the pyrolysis of part of the remaining organic matter. However, due to the low organic matter content of oil shale, the thermal decomposition at this stage was less pronounced compared with the low temperature stage, and the pyrolysis rate decreased significantly.

The pyrolysis of shale oil sludge on the other hand can be divided into three stages (Fig. 1b). In the first stage, at 50–200 °C, there was a rapid weight loss which was related to the evaporation of water and the release of light organic components from the sample. In the second stage, from 200 °C to 600 °C, mainly the heavy component was decomposed, and this stage was the principal stage of shale oil sludge pyrolysis. In the final stage, from 600 °C to 800 °C, there occurred the weight loss of semi-coke and mineral part. It was also at this stage that the final shale oil sludge product was rendered non-toxic.

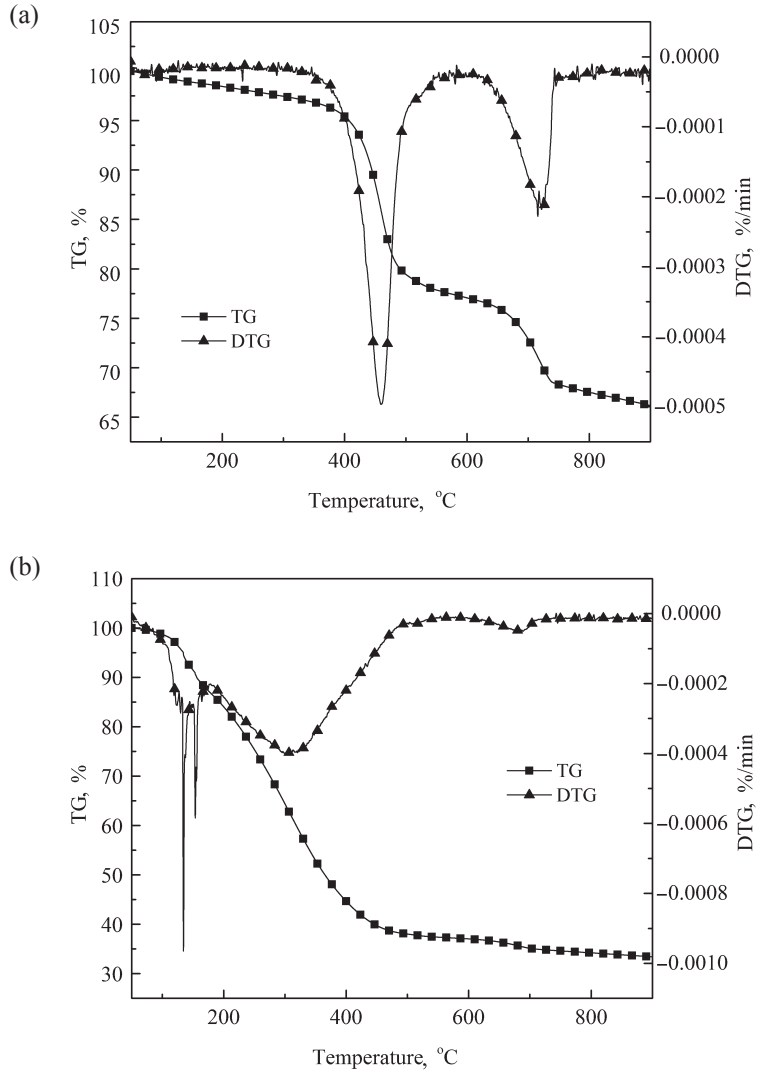

Fig. 1. TG-DTG curves of oil shale (a) and shale oil sludge (b).

3.2. Effect of mixing ratio

From the TG and DTG curves of mixed samples shown in Figures 2a and 2b at a heating rate of 10 °C/min, the weight loss peak in the DTG curve became higher with increasing proportion of sludge in the mixed sample, and the temperature corresponding to the maximum weight loss peak increased. The weight loss peak width also increased, indicating a longer pyrolysis time. When the sludge blending ratio was 80% or higher, the DTG curve had four weight loss peaks (Fig. 2b) most likely because the blending ratio was too high for the mixtures. The sludge dominated the pyrolysis process and the

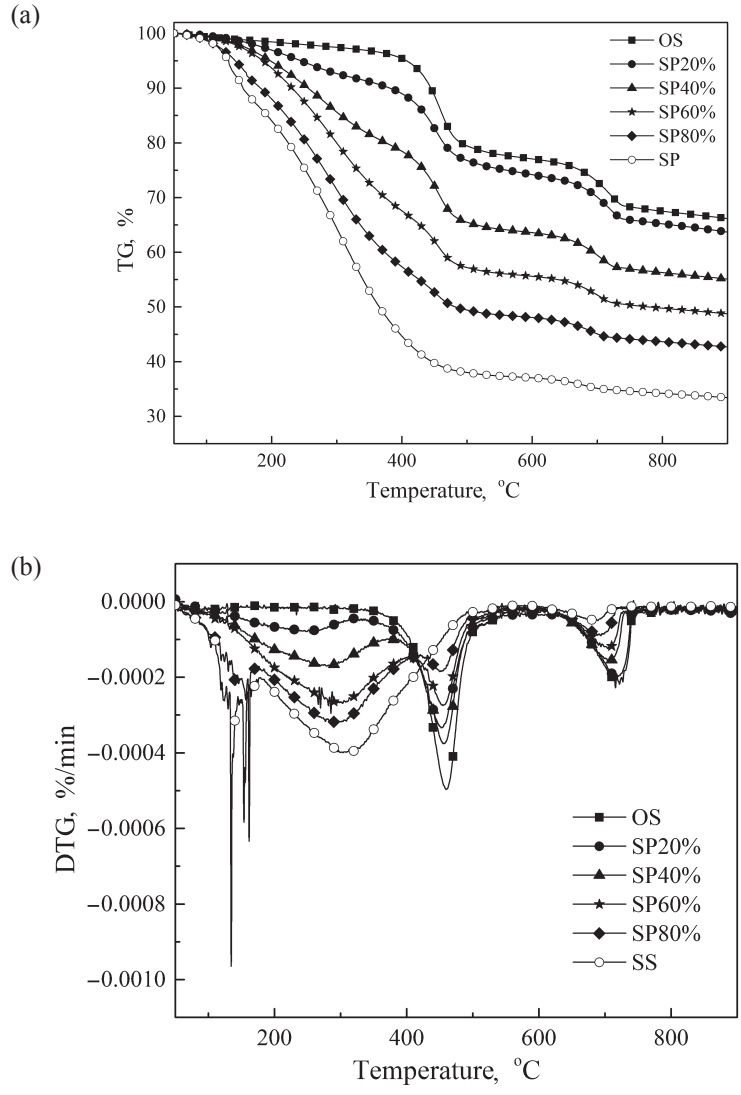

Fig. 2. TG (a) and DTG (b) curves of samples S_1 to S_6 at different mixing ratios.

spikes below 200 °C corresponded to the low temperature rise rate of moisture in the sludge and light components being freed from the sample.

The volatile components released at low temperatures are relatively simple, and the activation energy required for pyrolysis is low. After reaching their corresponding precipitation temperature, the pyrolysis products rapidly exhibit several discrete spikes. The three weight loss peaks appearing above 200 °C suggest the complicated composition of shale oil sludge in the sample and its higher oil content. With increasing mixing ratio, the mixture components are subjected to pyrolysis successively, i.e. first shale oil sludge is pyrolyzed and

then oil shale, giving a combination of two individual curves. These results are in agreement with the findings obtained by Ma and Sun [15] who studied the pyrolysis mechanism of shale oil sludge at linear heating temperature.

3.3. Effect of heating rate

The DTG curves of co-pyrolysis of oil shale and shale oil sludge generally exhibited the same evolution trend at different heating rates (Fig. 3). At different heating rates, the starting and ending reaction temperatures of each stage are slightly shifted towards the high temperature zone as the temperature increases. This is due to the fact that the pyrolysis of the sample is slow at the

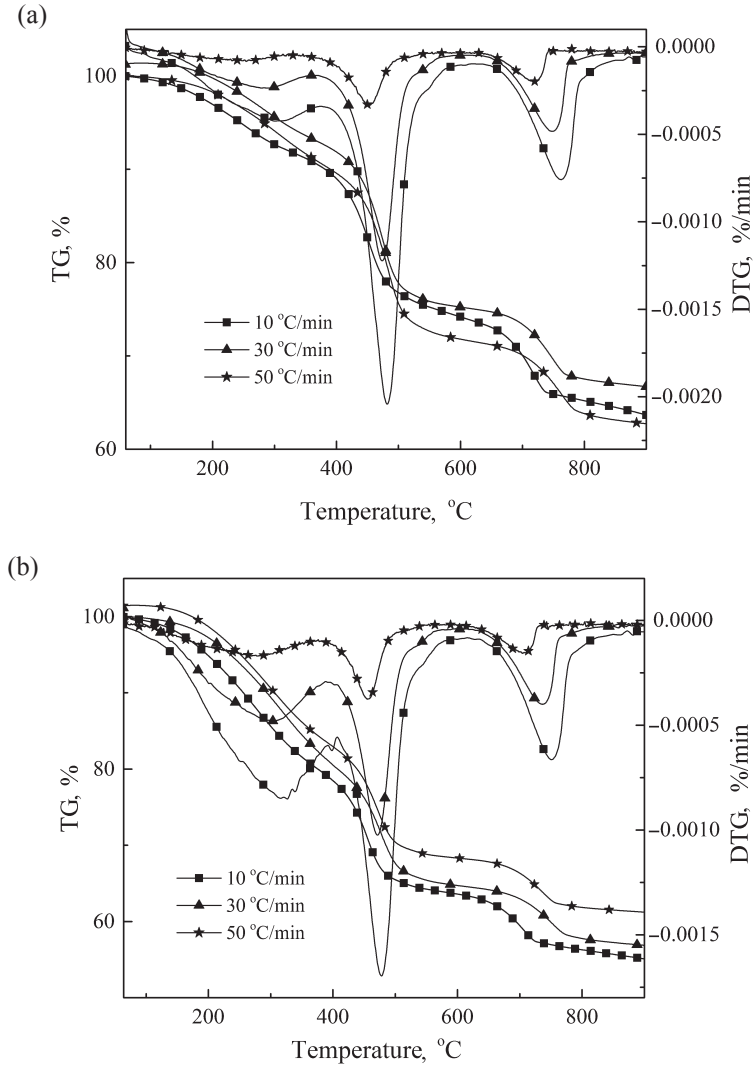

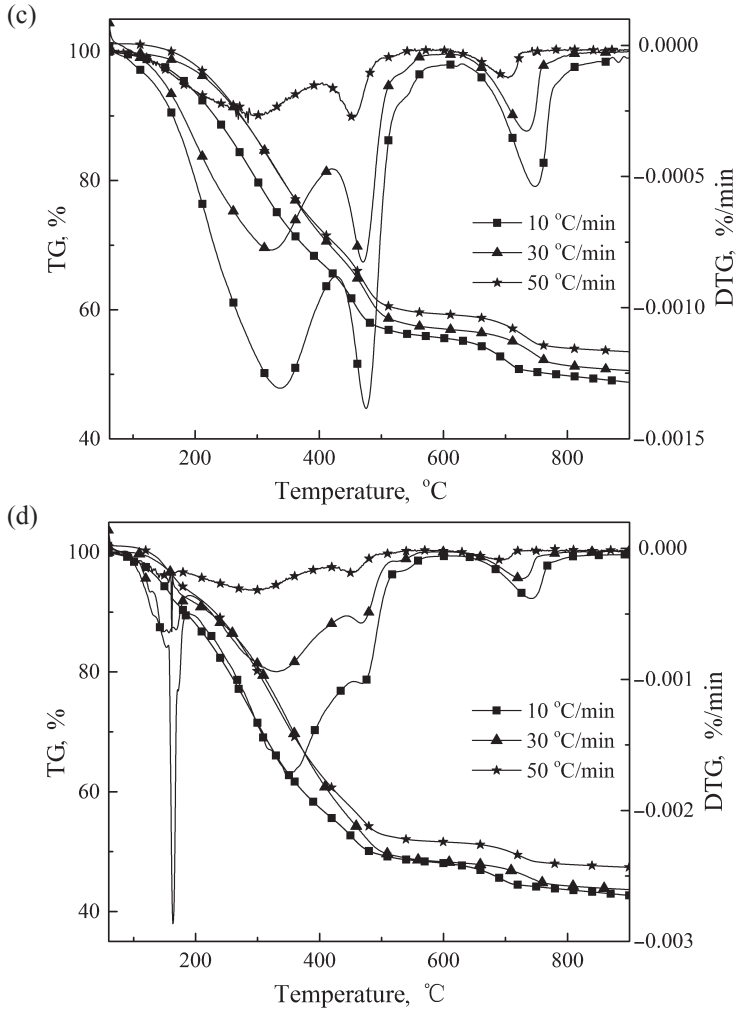

Fig. 3. TG and DTG curves of samples S_2 to S_5 at different heating rates: (a) S_2 (20% oil shale); (b) S_3 (40% oil shale); (c) S_4 (60% oil shale); (d) S_5 (80% oil shale).

beginning of the process when the rate of temperature increase is low, but at the end the sample is fully subjected to pyrolysis. But with increasing rate of temperature rise, the surface of the sample is completely subjected to pyrolysis, while its center is insufficiently heated to undergo pyrolysis. When the rate of temperature rise is too high, the sample does not fully undergo pyrolysis. This is particularly evident in the final stages of the process. Therefore, a lower heating rate is favourable for the complete pyrolysis of a sample, and the mass loss rate compared with that at 30 °C/min and 50 °C/min is also higher.

Furthermore, when the oil shale mixing ratio reached 80% (Fig. 3d), the co-pyrolysis was enhanced at all temperature changes compared to the other samples (Fig. 3a–c) due to the increase in the sludge content. The sludge is rich in water, and the water content of the mixed sample below 200 °C is high. The lower the rate of heating, the more complete the pyrolysis.

4. The mutual interaction between reactants during co-pyrolysis

RMS and *f* were used to analyze the synergistic effect of co-pyrolysis of oil shale and shale oil sludge. The pyrolysis of the mixture is not a simple pyrolysis of a single sample but a process of mutual influence of its components. The increasing mixing ratio does not necessarily mean an increase in synergistic effect, but rather its degrees are different. In the first stage of pyrolysis, the RMS value increased as the sludge ratio increased. In the second stage, RMS decreased compared to the first stage for 40%, 60% and 80% oil shale, indicating that the overall interaction between the reactants decreased (Table 3). During the last stage, the RMS value was stable as the sludge ratio increased. The *f* value for the first stage of pyrolysis for sample S_4 indicated that the co-pyrolysis process between oil shale and sludge was enhanced, while in case of sample S_2 its components exhibited mutual inhibiting effects. The co-pyrolysis processes of samples S_3, S_4 and S_5 were promoted. On the whole, it is advantageous to the pyrolysis to increase the ratio of the mixed sludge. However, when the proportion of sludge in the mixture is too high, oil shale and sludge mutually inhibit the process. The reason may be that the shale oil sludge composition is more complex and its oil content is higher, which in turn leads to the suppression of pyrolysis. This means that when the content of sludge in the mixed sample increases, it will stick to oil shale in large amounts, whereas the pyrolysis temperature of sludge is lower than that of oil shale, so, it is pyrolyzed at a lower temperature compared to oil shale. The gases released by pyrolysis increase the porosity of the mixture, thus boosting the process. When the sludge content of the mixture is too high, the amount of shale dust contained in the fine oil mist in the sludge is much higher than that of oil shale. As the temperature rises during pyrolysis, the sludge impedes the release of gas and indirectly increases the pyrolysis initiation temperature of oil shale. As a result, the entire process of pyrolysis of the sample is not sufficient with the sludge content being too high to play an inhibitory role.

Table 3. Synergy evaluation parameters of different blending samples

Sample (% SS)	First stage		Second stage		Third stage	
	f	RMS	*f*	RMS	*f*	RMS
S_2 (20%)	0.895	0.062	0.933	0.173	1.115	0.114
S_3 (40%)	0.928	0.258	1.242	0.107	1.127	0.332
S_4 (60%)	1.111	0.267	1.192	0.065	1.235	0.291
S_5 (80%)	0.936	0.114	0.987	0.073	1.152	0.271

SS – shale oil sludge.

5. FTIR analysis of pyrolysis gas

The flue gas from the pyrolysis of oil shale and shale oil sludge at 10 °C/min at various temperatures was analyzed by Fourier transform infrared spectroscopy (FTIR) (Fig. 4). Considering that the pyrolysis of oil shale occurred in two stages, its infrared shading analysis was carried out at four temperature points. The first stage of pyrolysis took place at 386–510 °C and the second stage from 620 °C to 714 °C; the spectra were analyzed at these specific temperature points – 386 °C, 510 °C, 620 °C and 714 °C (Fig. 4a). The spectra at different temperatures in Figure 4a show a complex characteristic peak, including some pyrolysis products with characteristic peaks. Based on the literature and infrared spectrum, the characteristic absorption peaks corresponded to NH_3 (930–946 cm^{-1}), carbonyl (1159 cm^{-1}), H_2O (1521 cm^{-1}), carboxyl (1764 cm^{-1}), CO (2110–2173 cm^{-1}), CO_2 (2358 cm^{-1}) and CH_4 (3014 cm^{-1}). Oil shale was pyrolyzed at 386 °C without releasing NH_3 and the amount of NH_3 reached the maximum at 510 °C (Fig. 4a). This was most likely because of the instability of heat transfer to the urea and amino acids with the release of a low amount of small ammonia molecules. The release of small amounts of carboxyl and carbonyl started at 510 °C. Water precipitated at 386 °C was mainly oil shale water and some of the escaping mineral crystal water. At 510 °C the precipitation of water reached its maximum. Pyrolysis of water was mainly due to the decomposition of oil shale oxygen-containing functional groups, such as phenolic hydroxyl and other fractions [16], while pyrolysis of mineral water was due to the dehydration of kaolinite, water mica and montmorillonite [17, 18]. CO was released during pyrolysis at 386 °C and this release continued to 620 °C, indicating that the temperature of CO precipitation was higher than 550 °C. CO was derived from oxygen-containing functional groups of oil shale other than the carboxyl group, such as ether bonds, phenols, heterocycles and short chain fatty acids [19]. In both pyrolysis stages, a significant CO_2 precipitation occurred, and as the temperature increased, the precipitation rate increased gradually. At this stage, the oil bond in the fat and some weak bonds of aromatic and oxygen-containing functional groups were broken. One portion of the broken carbonyl moiety was precipitated in the form of CO, while the other portion of it was bound to oxygen atoms in oil shale and precipitated as CO_2. CH_4 precipitated at each stage of pyrolysis and reached a maximum at 510 °C (Fig. 4). CH_4 was due to the fragmentation of aliphatic and aromatic side chains containing methyl functional groups.

The pyrolysis of shale oil sludge was divided into three stages, during which light volatile components quickly volatilized and heavy components rapidly and stably precipitated. The infrared spectra were analyzed at five temperature points. Shale oil sludge was mainly composed of shale dust, water and a small amount of oil (Table 1), while its composition was similar to that of oil shale except for the higher oil content. Therefore, with increasing temperature, the pyrolysis at different stages of water precipitation gradually progressed (Fig. 4b).

In the second stage, the gas precipitation water peak gradually decreased. The presence of a large amount of NH_3 in the second stage of pyrolysis might have led to the breakage of amino acids contained in shale oil sludge. Due to the high water content in the sludge and the semi-coke produced during pyrolysis, the sample easily reacted with water vapor at high temperatures. The reaction equation is as follows [20]:

$$CO + H_2O = CO_2 + H_2 \quad (11)$$

The characteristic peaks of CO are not very obvious. With the increase in temperature during the second and third stages, CO_2 was released more and more intensely. There was no significant release of carbonyl from the sludge. The gradual precipitation of the carboxyl group with the increase in temperature might be caused by the decomposition of proteins and cellulose in the sludge. The characteristic peaks of CH_4 revealed its significant precipitation at various stages of pyrolysis with increasing temperature, which then gradually decreased at 475 °C. This was mainly due to the semi-coke and hydrogen produced by pyrolysis to generate a large amount of methane:

$$C + 2H_2 = CH_4 \quad (12)$$

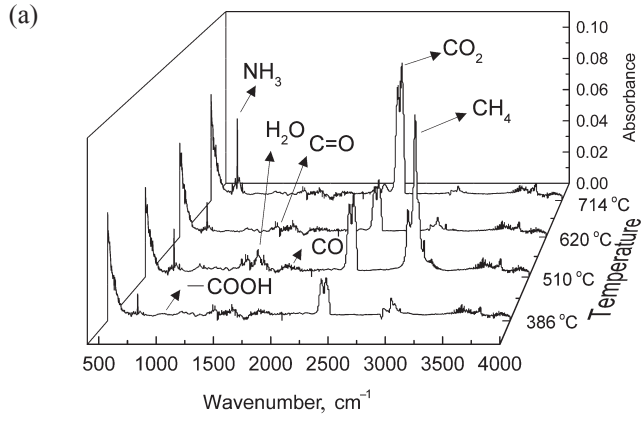

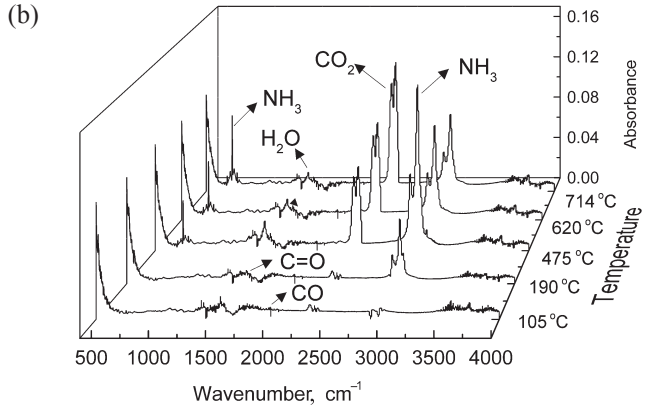

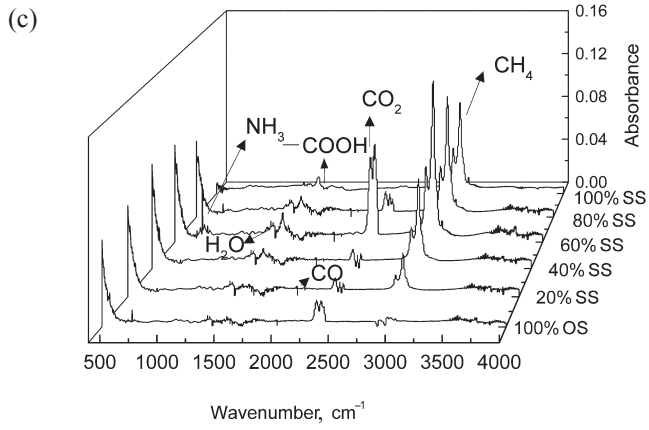

Fig. 4. Infrared spectra of pyrolysis gas from different samples: (a) pyrolysis of oil shale at a heating rate of 10 °C/min at several temperature snapshots; (b) pyrolysis of shale oil sludge at a heating rate of 10 °C/min at several temperature snapshots; (c) pyrolysis of samples S_2–S_5 at a heating rate of 10 °C/min and a temperature of 475 °C.

The effect of different mixing ratios on the infrared spectrum at a 10 °C/min heating rate in the most intensive pyrolysis reaction is shown in Figure 4c. With the increase in mixing ratio, the characteristic peak of H_2O gradually increased to its maximum at a mixing ratio of 60%. During the entire pyrolysis process, there was no significant increase in CO and carbonyl with increasing mixing ratio. The increase in the release of carboxyl, CO_2, CH_4 and NH_3 with the increase in mixing ratio was low, and when the mixing ratio was 60%, CO_2 as well as a large amount of NH_3 precipitated. The characteristic peaks of CO_2, CH_4 and NH_3 contained in pure sludge decreased again. These results show that with increasing sludge ratio, the characteristic peaks were not linearly related to the blending ratio. The incorporation of sludge is favorable for full pyrolysis, but its pyrolysis properties are not simple.

6. SEM analysis

Figure 5 shows SEM images of oil shale, pyrolysis sludge, pyrolysis oil shale and pyrolysis sample S_4 (60% oil shale) at three heating rates observed under the 5000x magnification. From the figure it can be seen that oil shale has a loose porous structure and there are some clearly visible pores in its surface. After the pyrolysis, the degree of fragmentation of the surface of the fault zone and the surface gap increased. During the pyrolysis, the surface of sludge is dense or porous, indicating that its structure is looser than that of oil shale.

At the same mixing ratio at the three heating rates the components of the mixture had contrasting micro-surface characteristics. At 10 °C/min, the sample surface structure is finer and has a clearly fractured zone, while at 30 °C/min, this is not so obvious. At 50 °C/min, the surface showed a coke-

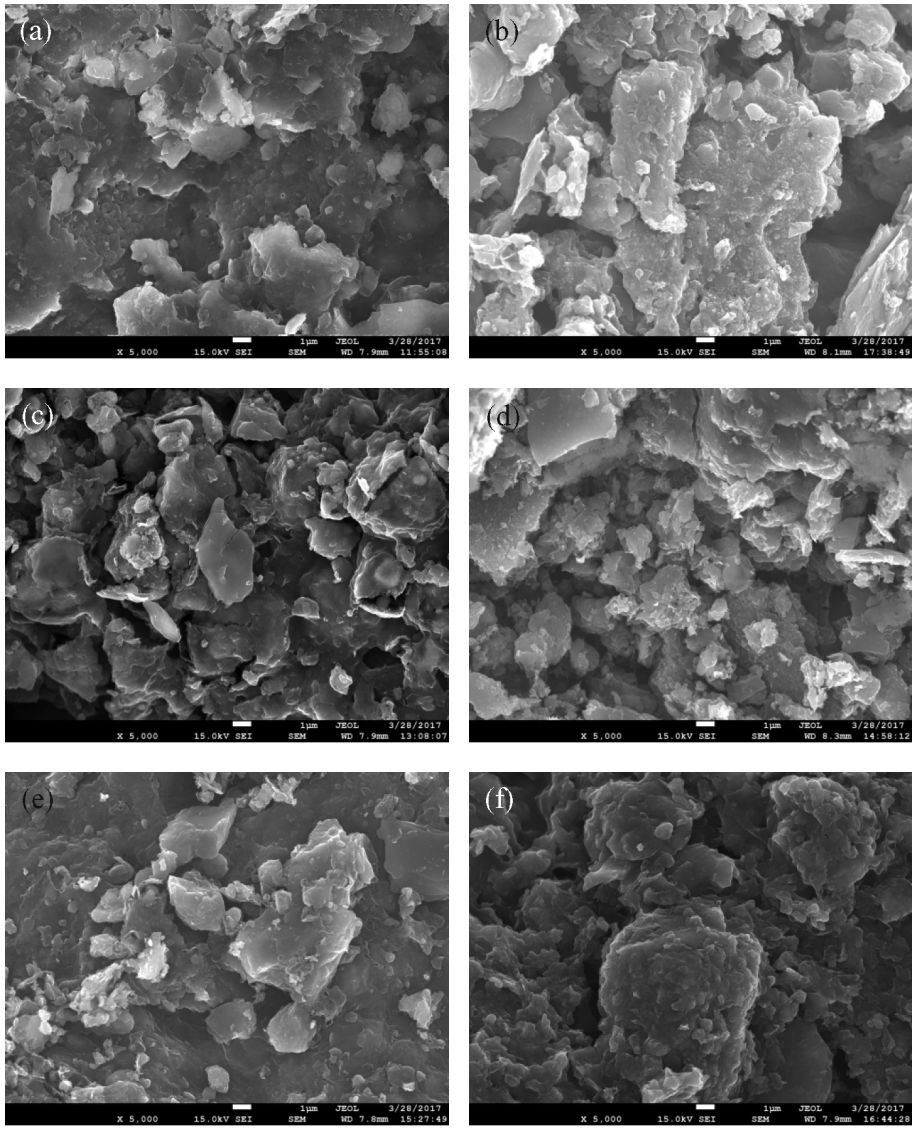

Fig. 5. SEM images of various samples: (a) oil shale; (b) pyrolysis sludge; (c) pyrolysis oil shale; (d) sample S_4 at 10 °C/min; (e) sample S_4 at 30 °C/min; (f) sample S_4 at 50 °C/min.

like structure, most likely because the order of the volatiles release from the sample during the pyrolysis changes its physical structure. The volatiles movement outwards leads to the formation of holes in the sample surface, which increases the surface area and the volume of pores. Secondary reactions occur during the precipitation process and a large number of secondary pores are formed, changing the pore size distribution.

7. Inorganic minerals analysis

The minerals contained in the sample may have either a positive or negative effect on pyrolysis. The energy spectrum analysis shows that most of the surface elements consist of carbonate and silicate minerals (Fig. 6). The alkali metals and alkaline earth metals in the carbonate form an alkaline earth metal-oxygen complex with the organic matter present in the sample. This complex provides active sites for pyrolysis reactions of oil shale, while at high temperatures silicate minerals along with alkali metals have a non-catalytic role for water insoluble compounds, which is just opposite to the effect of carbonate minerals. The reactions of silicates inhibit the decomposition of organic matter. This inhibition is stronger than the catalytic effect of alkaline earth metals. The same mixing ratio in the energy spectrum can be seen from the attribution of the elements at different heating rates. At 10 °C/min and 30 °C/min, the sample contains more carbonate than silicate, which promotes co-pyrolysis. At 50 °C/min, the case is opposite, the sample's silicate content is higher, therefore co-pyrolysis inhibits the pyrolysis process.

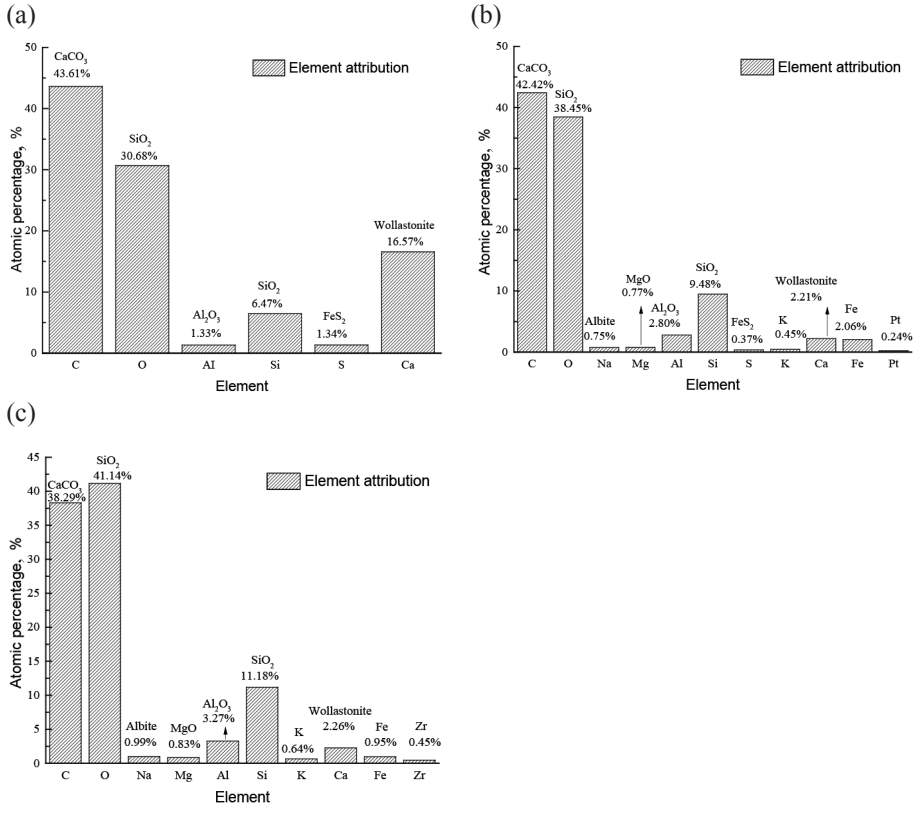

Fig. 6. Elemental analysis of sample S_4 at different heating rates: (a) 10 °C/min; (b) 30 °C/min; (c) 50 °C/min.

8. Specific surface area analysis

Figure 7a shows the specific surface area analysis of sample S_4 at a 60% mixing ratio and three heating rates. The adsorption and desorption curves of the sample were obtained from the graph. The desorption curve does not coincide with the adsorption curve to form a hysteresis loop, therefore the wider the hysteresis loop, the wider the pore distribution [21]. At a relative pressure P/P_0, the higher the degree of separation of the adsorption and desorption curves, the greater the corresponding pore amount [22]. It can be seen from Figure 7a that at 10 °C/min and 30 °C/ min the lag loop is wide, therefore the wide pore distribution is conducive to the pyrolysis of the sample. When the heating rate is 50 °C/min, the degree of separation of the adsorption and desorption curves of the sample is slightly lower, and the hysteresis loop is significantly smaller than at 10 °C/min and 30 °C/ min. This indicates that the amount of pores is reduced compared to that at lower heating rates. This finding confirms the results obtained by thermogravimetry and energy dispersive spectrometry.

Figure 7b shows the pore size distribution of oil shale after drying at different heating rates. The increase in the rate of heating after drying gradually reduces the total pore volume of the sample.. This may be explained by that the heating rate caused by the heat transfer of the sample was due to an uneven secondary cracking, followed by a gradual decline in pore size.

(a)

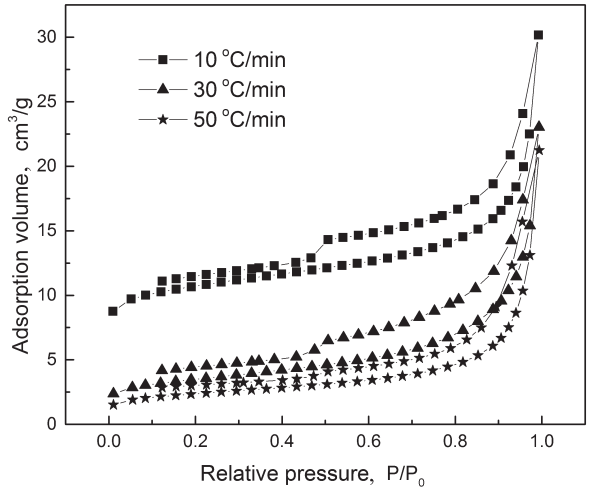

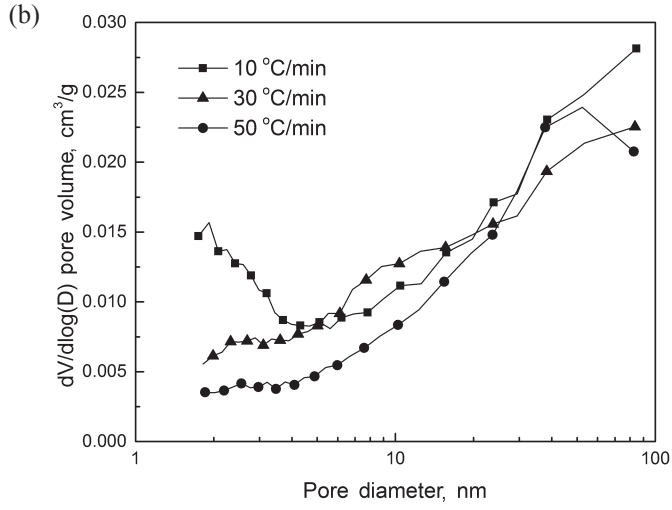

Fig. 7. Specific surface area analysis of sample S_4 at different heating rates.

9. The kinetic analysis of co-pyrolysis

Table 4 gives the kinetic parameters for samples of different mixing ratios.

Table 4. Calculated kinetic parameters for samples

Sample	β, °C/min	Temperature, °C	n	R	E, kJ/mol	A, min^{-1}
S_1	10	510–380	1	0.997	68.263	1574.192
	10	742–652	1	0.983	21.438	0.507
S_2	10	387–143	1	0.982	82.420	2755.395
	10	666–387	4	0.978	16.222	0.158
	10	756–666	7	0.970	36.810	9.746
S_3	10	374–129	7	0.993	72.384	2081.406
	10	615–374	7	0.988	23.358	2.834
	10	736–615	9	0.977	36.955	41.192
S_4	10	415–142	3	0.987	81.591	2504.243
	10	633–415	8	0.979	21.979	2.139
	10	727–633	8	0.974	36.532	57.247

Table 4 (continued)

S_5	10	430–183	4	0.996	64.003	1670.706
	10	615–430	7	0.974	20.960	3.570
	10	718–615	9	0.979	32.132	153.451
S_6	10	178–110	3	0.987	42.576	4731.418
	10	640–178	4	0.988	26.029	22.314
	10	708–640	7	0.977	16.068	13.103

As shown in Table 4, at different stages of pyrolysis, the reaction order n of oil shale pyrolysis is the same as that of the whole pyrolysis process, while the n and activation energy *E* of other reactions are different. This indicates that the co-pyrolysis of oil shale and shale oil sludge is a complex multi-step reaction process. The n and *E* of different samples are also different, therefore the pyrolysis mechanisms of different samples are different.

The pyrolysis of oil shale is divided into two stages based on the activation energy: the *E* of the early stage is higher than that in the later stage. This indicates that the oil shale pyrolysis is first difficult to proceed and requires a large amount of activation energy. Based on the results of infrared analysis obtained for oil shale oxygen-containing functional groups at a lower temperature, this may be explained by that oil shale mostly contains methyl functional groups. Numerous chemical bonds lead to the high temperature and activation energy of oil shale decomposition. In the high temperature zone, the pyrolysis reaction proceeds rapidly and the required amount of activation energy is low as the reaction progresses mainly due to the residual thermal stability of the side chains and the small amount of short chain fatty acids present. The apparent activation energy and frequency factor of sludge are found to be the same as those of oil shale. With the gradual reduction of activation energy, the reaction will progress more easily.

In the chemical reaction prior to pyrolysis, a large number of activated molecules were produced due to the intense molecular collision at this stage. There was mostly no activation energy between activated molecules in the chemical reactions, there was only a certain amount of relatively high energy between the reacting molecules. The reason for carrying out infrared analysis was that the decomposition of the internal moisture and some mineral water along with that of amino acids caused the escape of a significant amount of gases. In the pyrolysis, oil shale and sludge dominate the physical reaction of the pre-pyrolysis stage more than the chemical reaction. In the mixed sample, the moisture content in the sample increases with increasing sludge ratio, which leads to the increase of the temperature range and the activation energy of the first stage. The reason may be that as the proportion of sludge increases,

the moisture content of the mixed sample as well as the volatile content of the light component increases. The amount of activated molecules also increases, but the reaction of the mixed sample mainly occurs in the low temperature stage during the evaporation of water and light components. Therefore, the effective intermolecular collision at this stage of the chemical reaction is insignificant.

In the second stage of pyrolysis, the temperature range required for the process is gradually reduced. The major part of sludge is volatilized as the reaction progresses and the entire sludge wrap stage ends. Based on SEM and specific surface area analysis, the amount of sample surface pores increases and the diffusion of the internal gas becomes easier. When the required activation energy is reduced, at this stage organic matter begins to react adequately. In the third stage of pyrolysis, the temperature range does not change much and the pyrolysis reaction slows down with the increase in temperature. The activation energy at different mixing ratios is similar. This suggests that the pyrolysis reaction is close to completion at this stage. The activation energy required for each pyrolysis stage of the mixed sample first increases and with the depth of reaction decreases. This is indicative of that the co-pyrolysis has some synergistic effect unlike the individual pyrolysis of oil shale and shale oil sludge.

10. Conclusions

The conclusions about the study of co-pyrolysis of oil shale and shale oil sludge are summarized as follows:

The pyrolysis of the mixture of oil shale and shale oil sludge includes three stages: 1) escape of water and light components; 2) release of volatile gases; 3) decomposition of heavy components and organic matter.

Increasing the heating rate can effectively shorten the reaction time of the sample, however, this is not conducive to the completion of the pyrolysis. Increasing the sludge content promotes the decomposition of the mixture until its proportion reaches 60%.

Based on kinetic calculations, the activation energy of the mixture gradually increases with the degree of the reaction, while the frequency factor gradually decreases with the depth of the reaction. Therefore, the co-pyrolysis has an optimum reaction temperature interval and the degree of reaction is related to the chemical reaction between the reactants. This main co-pyrolysis temperature range is 374–666 °C.

Acknowledgement

The authors are grateful for the support from Jilin Science and Technology Development Plan Project (20150204012SF). This research was also supported by Jilin Provincial Department of Education Projects (2015, No. 251), National Natural Science Foundation of China (Grant No. 5167060959) and Changjiang Scholars Program (IRT_17R19).

REFERENCES

1. Hou, X. L. *Shale Oil Industry of China*. Petroleum Industry Press, Beijing, 1984 (in Chinese).
2. Peng, X., Ma, X., Lin, Y., Guo, Z., Hu, S., Ning, X., Cao, Y., Zhang, Y. Co-pyrolysis between microalgae and textile dyeing sludge by TG–FTIR: Kinetics and products. *Energ. Convers. Manage.*, 2015, **100**, 391−402.
3. Bičáková, O., Straka, P. Co-pyrolysis of waste tire/coal mixtures for smokeless fuel, maltenes and hydrogen-rich gas production. *Energ. Convers. Manage.*, 2016, **116**, 203−213.
4. Bozkurt, P. A., Tosun, O., Canel, M. The synergistic effect of co-pyrolysis of oil shale and low density polyethylene mixtures and characterization of pyrolysis liquid. *J. Energy Inst*., 2017, **90**(3), 355−362.
5. Lin, Y., Liao, Y., Yu, Z., Fang, S., Lin, Y., Fan, Y., Peng, X., Ma, X. Co-pyrolysis kinetics of sewage sludge and oil shale thermal decomposition using TGA–FTIR analysis. *Energ. Convers. Manage.*, 2016, **118**, 345−352.
6. Bai, J., Shao, J., Li, M., Jia, C., Wang, Q. Co-pyrolysis characteristic and dynamic analysis of alkali lignin and oil shale. *Transactions of the Chinese Society of Agricultural Engineering*, 2016, **32**(7), 187−193.
7. Liu, X. R., Lü, Q. G., Jiao, W. H. Thermogravimetric analysis of co-pyrolysis of coal with different municipal sewage sludge. *J. Fuel Chem. Technol*., 2011, **39**(3), 8−13.
8. Huang, Y. F., Shih, C. H., Chiueh, P. T., Lo, S. L. Microwave co-pyrolysis of sewage sludge and rice straw. *Energy*, 2015, **87**, 638−644.
9. Martínez, J. D., Veses, A., Mastral, A. M., Murillo, R., Navarro, M. V., Puy, N., Artigues, A., Bartroli, J., Garcia, T. Co-pyrolysis of biomass with waste tyres: Upgrading of liquid bio-fuel. *Fuel Process. Technol*., 2014, **119**, 263−271.
10. Ding, H. S., Jiang, H. Self-heating co-pyrolysis of excessive activated sludge with waste biomass: energy balance and sludge reduction. *Bioresource Technol*., 2013, **133**, 16−22.
11. Özveren, U., Özdoğan, Z. S. Investigation of the slow pyrolysis kinetics of olive oil pomace using thermo-gravimetric analysis coupled with mass spectrometry. *Biomass Bioener*., 2013, **58**, 168−179.
12. Hilten, R. N., Vandenbrink, J. P., Paterson, A. H., Feltus, F. A., Das, K. C. Linking isoconversional pyrolysis kinetics to compositional characteristics for multi-

ple Sorghum bicolor genotypes. *Thermochim. Acta*, 2014, **577**, 46–52.
13. Jiang, Z., Liu, Z., Fei, B., Cai, Z., Yu, Y., Liu, X. The pyrolysis characteristics of moso bamboo. *J. Anal. Appl. Pyrol*., 2012, **94**, 48–52.
14. Mu, L., Chen, J., Yin, H., Song, X., Li, A., Chi, X. Pyrolysis behaviors and kinetics of refining and chemicals wastewater, lignite and their blends through TGA. *Bioresource Technol*., 2015, **180**, 22–31.
15. Ma, B., Sun, B. Pyrolysis mechanism of shale oil sludge under linear heating temperature. *Chemical Industry and Engineering Progress*, 2013, 7–13 (in Chinese).
16. Linder, G., Andersson, L. A., Bjerle, I. Influence of heating rate on the pyrolysis of oil shale. *Fuel Process. Technol*., 1983, **8**(1), 19–31.
17. Charland, J.-P., MacPhee, J. A., Giroux, L., Price, J. T., Khan, M. A. Application of TG-FTIR to the determination of oxygen content of coals. *Fuel Process. Technol*., 2003, **81**(3), 211–221.
18. Wang, Q., Wang, R., Jia, C., Ren, L., Yan, Y. FG-DVC model for oil shale pyrolysis. *CIESC Journal*, 2014, **65**(6), 2308–2315 (in Chinese, summary in English).
19. Zhao, L., Guo, H., Ma, Q. Study on gaseous products distributions during coal pyrolysis. *Coal Conversion*, 2007, **30**(1), 5–9.
20. Ma, B. *Study on the Pyrolysis Properties of Shale Oil Sludge*. PhD Dissertation, Northeast Dianli University, 2013.
21. Schrodt, J. T., Ocampo, A. Variations in the pore structure of oil shales during retorting and combustion. *Fuel*, 1984, **63**(11), 1523–1527.
22. Qi, H., Ma, J., Wong, P. Adsorption isotherms of fractal surfaces. *Colloid. Surface. A*., 2002, **206**(1–3), 401–407.

Presented by A. Siirde
Received January 17, 2019